Anisotropic Vortex Squeezing in Synthetic Rashba Superconductors: A Manifestation of Lifshitz Invariants

L. Fuchs,[1] D. Kochan,[2,3] J. Schmidt,[1] N. Hüttner,[1] C. Baumgartner,[1] S. Reinhardt,[1] S. Gronin,[4] G. C. Gardner,[4] T. Lindemann,[5,4] M. J. Manfra,[4,5,6,7] C. Strunk,[1] and N. Paradiso[1,*]

[1]*Institut für Experimentelle und Angewandte Physik, University of Regensburg, 93040 Regensburg, Germany*
[2]*Institut für Theoretische Physik, University of Regensburg, 93040 Regensburg, Germany*
[3]*Institute of Physics, Slovak Academy of Sciences, 84511 Bratislava, Slovakia*
[4]*Birck Nanotechnology Center, Purdue University, West Lafayette, Indiana 47907, USA*
[5]*Department of Physics and Astronomy, Purdue University, West Lafayette, Indiana 47907, USA*
[6]*School of Materials Engineering, Purdue University, West Lafayette, Indiana 47907, USA*
[7]*School of Electrical and Computer Engineering, Purdue University, West Lafayette, Indiana 47907, USA*

(Received 4 March 2022; revised 25 July 2022; accepted 28 September 2022; published 21 November 2022)

Epitaxial superconductor-semiconductor heterostructures combine superconductivity with strong spin-orbit interaction resulting in synthetic Rashba superconductors. The theoretical description of such superconductors involves Lifshitz invariants that are predicted to feature numerous exotic effects with so far sparse experimental evidence. Using a new observable—vortex inductance—we investigate the pinning properties of epitaxial Al/InAs-based heterostructures. We find a pronounced *decrease* of the vortex inductance with increasing in-plane field which corresponds to a counterintuitive increase of the pinning force. When rotating the in-plane component of the field with respect to the current direction, the pinning interaction turns out to be highly anisotropic. We analytically demonstrate that both the pinning enhancement and its anisotropy are consequences of the presence of Lifshitz invariant terms in the Ginzburg-Landau free energy. Hence, our experiment provides access to a fundamental property of Rashba superconductors and offers an entirely new approach to vortex manipulation.

DOI: 10.1103/PhysRevX.12.041020

Subject Areas: Condensed Matter Physics, Superconductivity

Breaking the inversion symmetry in superconductors has numerous important consequences [1–3]. Often it occurs through the Rashba spin-orbit interaction (SOI) which spin splits the Fermi surface and links the electron spin to the momentum. If the SOI is strong enough to compete with the superconducting pairing, it gives rise to plenty of interesting phenomena, such as, e.g., singlet-triplet mixing [4,5], unconventional pairing [6–9], Ising superconductivity [10,11], magnetochiral resistance [12–16], anomalous Josephson effect [17–27], supercurrent diode effect [28–30], topological superconductivity [31–33], and helical phases [34–36] with a spatially modulated order parameter.

One possibility to engineer *synthetic* 2D Rashba superconductors consists in proximitizing a 2D electron gas (2DEG) with large Rashba SOI by a standard *s*-wave superconductor. This can be realized, e.g., by epitaxially growing an Al film on a shallow InAs quantum well [37–40]. Owing to their nontrivial topological features [6,31,41], such hybrid 2D semiconductor-superconductor heterostructures have been intensely investigated. So far, theory and experiments are mainly aimed at exploring the Majorana modes at the edge of topological superconductors, which is enabled by the bulk-boundary correspondence [42–48]. In contrast, experimental signatures of the impact of SOI on the superfluid condensate as such are rather sparse in hybrid systems [9].

Besides the microscopic description in terms of the Bogoliubov–de Gennes or Gor'kov equations, the effects of SOI and magnetic field on the superconducting condensate can be accounted for phenomenologically by adding new terms into the underlying Ginzburg-Landau free energy. Such terms—called *Lifshitz invariants* [36,49,50]—depend on the crystal point-group symmetry [3] and, in the simplest case, they form triple products of magnetic field, linear spatial gradient of the order parameter, and a vector specified by SOI. The presence of the Lifshitz invariants is theoretically predicted to lead to an anisotropic response of the superflow and gives rise to

*nicola.paradiso@physik.uni-regensburg.de

magnetoelectric effects [51,52], helical phases [53–55], anomalous magnetization [56,57], vortex lattice reorientation [58], and anomalous φ_0 shift in Josephson junctions [18]. To our knowledge, there are so far no experimental evidences of the Lifshitz invariant.

Vortices can be used to probe the structure of the order parameter $\Psi(x,y)$, because $|\Psi(x,y)|^2$ near the vortex core is proportional to the potential $U(\mathbf{r})$ that confines a vortex near a pointlike pinning site, with $\mathbf{r}=(x,y)$ being the vortex displacement from the pinning center at (x_0,y_0); see Fig. 1(a) [59]. In parabolic approximation the potential $U(\mathbf{r}) \simeq k\mathbf{r}^2/2$ is characterized only by its curvature k [61]. Driving vortex oscillations around the pinning centers with an ac current leads to an inductive voltage response, i.e., a vortex inductance,

$$L_v = N_\square \frac{B_z \Phi_0}{k}, \tag{1}$$

where B_z is the out-of-plane magnetic field, $\Phi_0 = h/(2e)$ the superconducting flux quantum, and $N_\square = l/w$ is the ratio of length l and width w of the film [62–64].

In this work, we demonstrate an unusual, anisotropic *decrease* of the vortex inductance when varying the magnitude and spatial orientation of the in-plane magnetic field. We interpret this observation as an experimental

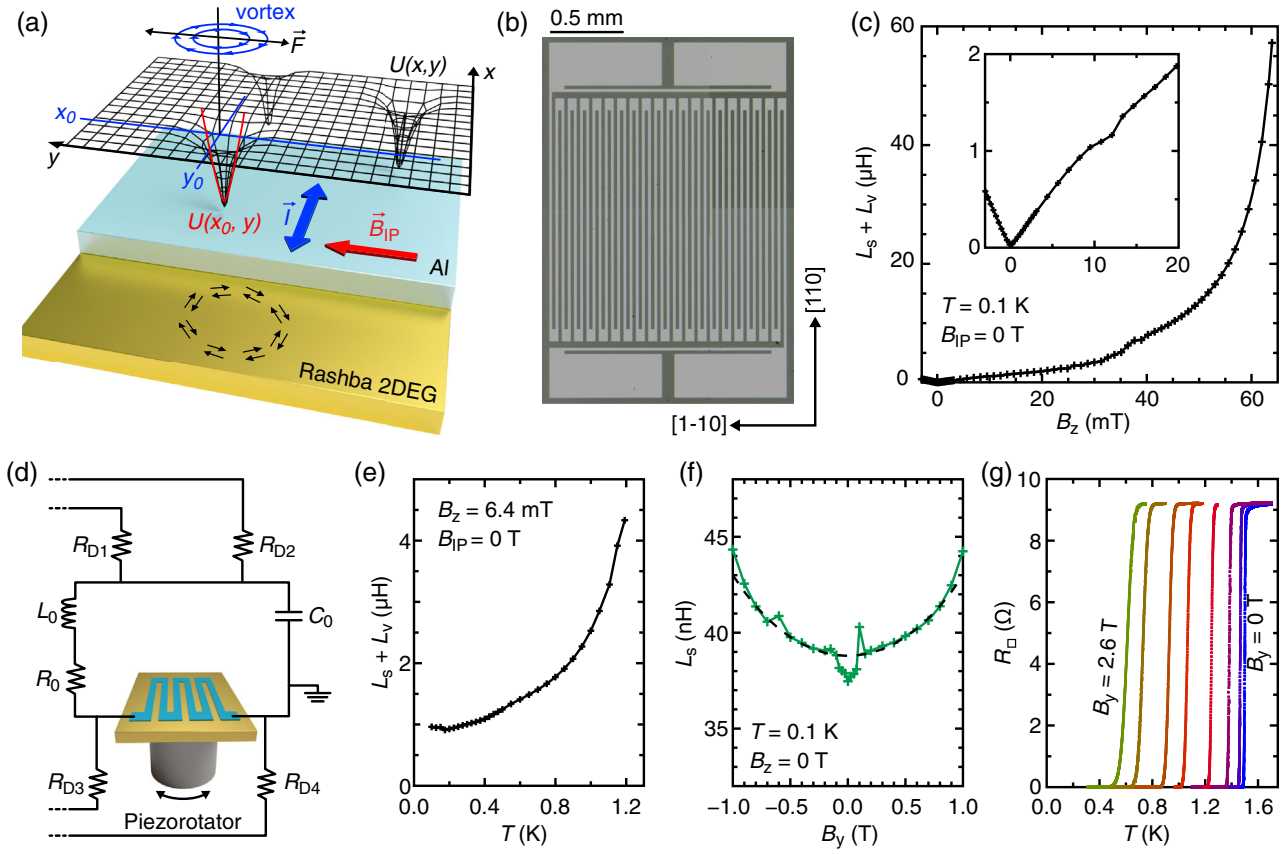

FIG. 1. Vortex inductance as a probe of the pinning potential. (a) Sketch of the device under study. An epitaxial Al film (light blue) proximitizes from the top a shallow InAs quantum well (yellow). The sample is patterned as a 24-μm-wide and 7.3-cm-long meander [see micrograph in (b)]. The current flows mainly along the $\hat{\mathbf{x}}$ direction, and is subjected to a vortex-generating out-of-plane magnetic field B_z and an in-plane field $\mathbf{B}_{IP} \equiv B_x\hat{\mathbf{x}} + B_y\hat{\mathbf{y}}$ at a variable angle θ with respect to the $\hat{\mathbf{x}}$ axis, which can be controlled. The grid represents the vortex free energy $U(x,y)$ for displacement from the pinning centers. An ac current $\mathbf{I}\|\hat{\mathbf{x}}$ exerts Lorentz force $\mathbf{F}\|\hat{\mathbf{y}}$. The restoring potential in harmonic approximation (small oscillations) is $U(x_0,y) = k_y(y-y_0)^2/2$ (red parabola), with $k_y = \partial_y^2 U(x_0,y_0)$. (b) Optical micrograph of the sample. Light gray area corresponds to the Al film, while the dark green ones are etched down to the mesa. (c) Vortex (L_v) plus kinetic (L_s) inductance as a function of B_z. In our samples L_s (≈40 nH; see next panel) is negligible compared to L_v. The graph shows that by increasing the vortex density, the inductance increases. At low fields (inset) the increase is linear, see Eq. (1). At larger vortex densities, the increase is superlinear owing to pair breaking, which leads to divergence at $B_{c2} = 61$ mT. (d) Measurement scheme: the sample is embedded in a *RLC* circuit at low temperature and can be rotated with respect to $\mathbf{B}_{IP}$ by means of a piezorotator. (e) Measured inductance for $B_z = 6.4$ mT as a function of temperature. (f) Kinetic inductance versus B_y for $B_x = B_z = 0$. (g) Temperature dependence of the sheet resistance measured at $B_x = B_z = 0$ for (right to left) $B_y = 0$, 0.5, 1, 1.5, 2, 2.25, 2.5, 2.6 T.

signature for the so far elusive Lifshitz invariant terms in the Ginzburg-Landau equations for $\Psi(x, y)$. In the presence of an in-plane field, an enhancement of the pinning force is observed that reflects an elliptic contraction of the order parameter profile. Such pinning enhancement is hard to explain by other known mechanisms, and offers a direct insight into the unusual structure of the order parameter near the vortex cores of Rashba superconductors.

Figure 1(a) shows a schematic of the pinning landscape $U(x, y)$ for a pinned vortex together with the directions of in-plane magnetic field and the ac drive current. A supercurrent in the x direction generates a Lorentz force that displaces vortices in the y direction from their equilibrium positions. This increases the free energy, producing a restoring force. For small displacements and low frequencies, pinned vortices thus behave as underdamped harmonic oscillators [62–64].

Our synthetic Rashba superconductor is fabricated starting from a InAs/InGaAs quantum well capped by an epitaxial Al film of nominal thickness $d = 7$ nm [65]. The Al film induces superconducting correlations in the shallow 2DEG by proximity effect. The penetration depth λ and the coherence length ξ for the Al-2DEG system at 100 mK are 227 and 73 nm, respectively [66]. Using optical lithography and wet etching, we pattern a meander structure, as depicted in Fig. 1(b). The meander is 24 μm wide, which is larger than the Pearl penetration depth $\lambda_\perp = 2\lambda^2/d = 8$ μm, and a total length of 7.3 cm, resulting in $N_\square = 3042$ squares. These dimensions are motivated by the need of having at the same time a device in the 2D regime and a large number of squares to increase the measured vortex and kinetic inductance.

The sample holder is mounted on a piezorotator, whose rotation axis is parallel to the $\hat{\mathbf{z}}$ axis, i.e., perpendicular to the film. A superconducting coil provides an in-plane magnetic field parallel to the $\hat{\mathbf{y}}$ axis, while an orthogonal pair of coils provides a small out-of-plane field in the $\hat{\mathbf{z}}$ direction. The device under study is embedded in a RLC resonant circuit located on the sample holder; see Fig. 1(d). The circuit, described in Ref. [65], allows us to simultaneously measure dc transport characteristics and sample inductance. The latter is deduced from the center frequency shift of the RLC resonance spectrum, which is measured by lock-in detection in the few megahertz regime. This is far below the characteristic frequency $\omega_0/2\pi = R_N/2\pi L_v \simeq 4.6$ GHz (R_N being the normal state resistance) [63,64] that separates inductive and dissipative regimes [67]. In our inductance measurements we apply a maximum ac excitation of 10 μV to one of the decoupling resistors, namely, R_{D1}; see Fig. 1(d). This corresponds to an ac current of 10 nA at low frequency and roughly 350 nA near the resonance, 3 orders of magnitude less than the critical current. In this regime, all the results here shown are independent of the excitation amplitude.

Figure 1(c) shows how the sample inductance depends on the out-of-plane magnetic field B_z. We notice that the function $L_v(B_z)$ is nearly linear up to 20 mT (corresponding to $B_z \approx B_{c2}/3$), indicating that the inductance per added vortex is approximately constant. This means that the interaction between vortices is not relevant in this regime. The measured ratio $L_v/B_z = 118$ nH/mT is of the same order as the value expected from Eq. (1) for a reasonable estimate of k [66]. At fields higher than 20 mT, the B_z dependence of the vortex inductance increases faster than linear [Fig. 1(c)]. In this regime, the order parameter in between the close-packed vortices is reduced compared to unperturbed value far from an isolated vortex. Hence, the curvature k of $U(x, y)$ is reduced as well, leading to a superlinear dependence of L_v on B_z.

More generally, any pair-breaking mechanism tends to reduce the curvature k. As another example, Fig. 1(e) shows the temperature dependence of the vortex inductance at $B_z = 6.4$ mT [linear low-field regime in Fig. 1(c)]. A pronounced increase of the vortex inductance is observed, which becomes very steep when the critical temperature is approached. Finally, pair breaking by a purely in-plane field $\mathbf{B}_{\mathrm{IP}} \equiv B_x\hat{x} + B_y\hat{y}$ must be reflected in the pure kinetic inductance L_s too. This measurement is shown in Fig. 1(f), where the in-plane field is directed along the y direction. Note the scale of the vertical axis: the kinetic inductance is 25 times smaller than the vortex inductance at 10 mT, and it varies by only few nanohenry for applied fields of the order of 1 T [68]. The sharp minimum for $|B_y| < 100$ mT is likely due to the suppressed contribution of the Al wires used to bond the sample on the chip carrier. Orbital pair breaking is also seen in Fig. 1(g), which displays a reduction of $T_c(B_y)$ in $R(T, B_y)$ measurements.

Having established the vortex inductance as a sensitive probe of the pinning strength k, we now come to our main observation, namely, an entirely unexpected *increase* of the pinning strength controlled by the in-plane magnetic field. Figure 2(a) shows L_v versus B_{IP} at $B_z = 10$ mT [linear regime in Fig. 1(c)], for both $\mathbf{B}_{\mathrm{IP}}$ parallel (blue) and perpendicular (red) to the direction of the drive current $\mathbf{I} \equiv dw\mathbf{j}$, where the current density vector $\mathbf{j}$ is oriented along $\hat{\mathbf{x}}$, corresponding to the [110] direction of InAs [Fig. 1(b)]. In stark contrast to the behavior at $\mathbf{B}_z = 0$ [Fig. 1(f)], a drastic and surprising *suppression* of the vortex inductance is seen for both orientations when B_{IP} is increased. At very high magnetic fields exceeding 2 T, the inductance reaches a minimum and increases again near the in-plane critical field $B_{c,IP} \approx 2.7$ T, where it is expected to diverge. The full angle dependence of $L_v(\theta)$ is displayed in Fig. 2(b) for $B_z = 0$, 2, 5, and 10 mT. The blue curve in Fig. 2(b) corresponds to the absence of vortices; i.e., the measured inductance is the kinetic inductance of the superfluid. The red curve in Fig. 2(b) corresponds to the same vortex density as in Fig. 2(a). While the kinetic inductance is nearly isotropic at $B_{\mathrm{IP}} = 0$ [66], the vortex inductance shows a pronounced θ dependence with a twofold symmetry. In order to confirm that the effect

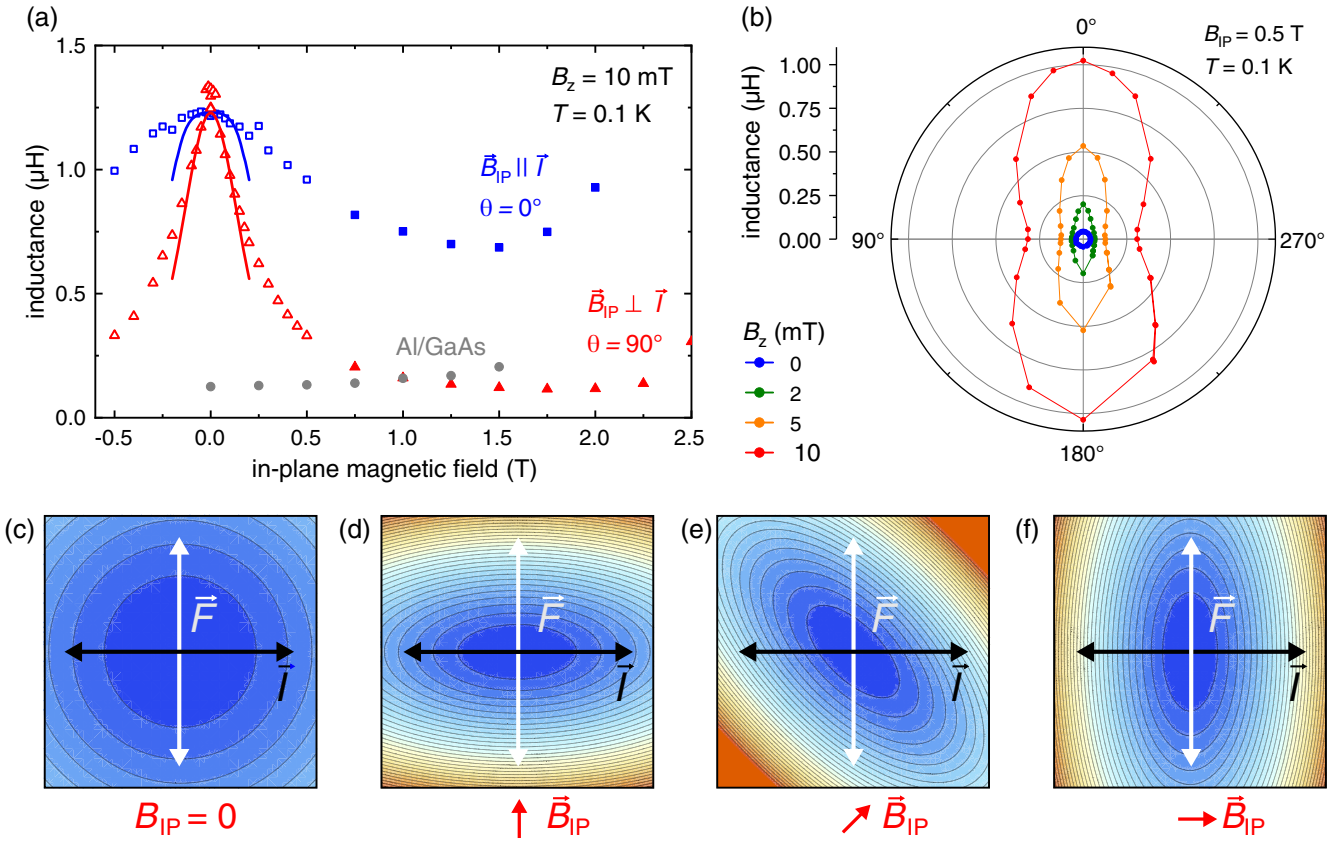

FIG. 2. Anisotropic vortex squeezing under in-plane field. (a) Sample inductance measured at $T = 0.1$ K as a function of B_{IP} for $\mathbf{B}_{IP} \| \hat{\mathbf{x}}$ ($\theta = 0°$, blue symbols) and for $\mathbf{B}_{IP} \| \hat{\mathbf{y}}$ ($\theta = 90°$, red symbols). The out-of-plane field $B_z = 10$ mT corresponds to the linear regime in Fig. 1(c). Empty and full symbols refer to two measurement sessions with higher resolution at low fields and lower resolution at high fields, respectively. We also report the results (gray symbols) of the control measurement performed on a sample with epitaxially grown Al on intrinsic GaAs. The solid red (blue) curve is obtained by fitting the experimental data for $\mathbf{B}_{IP} \perp \mathbf{I}$ ($\mathbf{B}_{IP} \| \mathbf{I}$) to the analytical model; see text. (b) Polar plot showing the angle θ dependence of the vortex inductance for selected values of B_z. (c) The color plot schematically represents the modulus of the order parameter $|\Psi(x, y)|^2$ near the core of a pinned vortex, in the absence of in-plane field B_{IP}. The horizontal black arrow represents the direction of an oscillating current bias $\mathbf{I} \| \hat{\mathbf{x}}$, which exerts a Lorentz force $\mathbf{F} \| \hat{\mathbf{y}}$, white arrow. The measured vortex inductance is rotation symmetric and inversely proportional to the curvature of $|\Psi(x, y)|^2$ along $\mathbf{F}$. (d) When a finite in-plane field is applied along $\hat{\mathbf{y}}$, the vortex core is squeezed as a consequence of the Rashba spin-orbit interaction. In this plot the curvature k_x (k_y) along the x axis (y axis) is 1.64 (7.66) times that shown in (c), reflecting the measured change in vortex inductance for $B_{IP} = 1$ T; see text. The curvature is always probed along $\mathbf{F} \| \hat{\mathbf{y}}$. (e),(f) By rotating $\mathbf{B}_{IP}$ clockwise, the anisotropic vortex core rotates accordingly. Since the $\mathbf{F}$ direction stays constant, such rotation makes it possible to probe the curvature of $|\Psi(x, y)|^2$ along an arbitrary direction and thus to extract its spatial tomography. The color range and level spacing is arbitrary, but the same in all the color plots.

results from SOI in the InAs quantum well, we have performed a control measurement on an Al film grown epitaxially on GaAs. There is no 2DEG in GaAs and hence superconductivity is confined to the Al film. Moreover, in GaAs SOI is much smaller than in InAs, even when considering the effect of the Al/GaAs interface. For this device, the measured vortex inductance gradually increases with increasing in-plane field; see gray symbols in Fig. 2(a). Importantly, this increase is almost perfectly isotropic [66].

Figures 2(c)–2(f) illustrate the order parameter profiles $|\Psi(x, y)|^2$ near the vortex cores as inferred from the measured reduction of the vortex inductance. Figure 2(c) shows $|\Psi(x, y)|^2 \propto U(x, y)$ in the vicinity ($x^2 + y^2 \ll \xi^2$) of the vortex center for $\mathbf{B}_{IP} = 0$. The vortex is assumed to be pinned at a point defect located at the center of the figure. Since nothing breaks isotropy, the contours of constant $|\Psi(x, y)|^2$ are circles. As discussed above, the corresponding inductive voltage response reflects the curvature k_y of $|\Psi(x, y)|^2$ along $\hat{\mathbf{y}}$.

If an additional in-plane field is applied, e.g., along $\hat{\mathbf{y}}$ [$\theta = 90°$, Fig. 2(d)], the vortex core will be squeezed in both the $\hat{\mathbf{x}}$ and the $\hat{\mathbf{y}}$ direction. However, the effect is more pronounced for the direction along $\mathbf{B}_{IP}$ (in this case $\hat{\mathbf{y}}$); i.e., $\partial_y^2 U(x, y) > \partial_x^2 U(x, y)$. Thus, for $\mathbf{B}_{IP} > 0$ the contour lines of constant $|\Psi(x, y)|^2$ become ellipses with minor axis

directed along $\mathbf{B}_{\mathrm{IP}}$. By rotating $\mathbf{B}_{\mathrm{IP}}$, the elliptic core will rotate accordingly. Such anisotropic vortex squeezing is the main result of our work. It is important to stress that it is the in-plane field $\mathbf{B}_{\mathrm{IP}}$ that breaks the rotational symmetry. On the other hand, to *detect* such anisotropy in the experiment, we use the supercurrent direction ($\hat{\mathbf{x}} \| \mathbf{I}$) as a reference. Since in our device vortices oscillate along the $\hat{\mathbf{y}} \perp \mathbf{I}$ direction, the largest curvature $k_{\perp}$ (i.e., the smallest inductance) is probed for $\mathbf{B}_{\mathrm{IP}} \perp \mathbf{I}$ [$\theta = 90°$, Fig. 2(d)] while the smallest curvature $k_{\parallel}$ (largest inductance) is probed for $\mathbf{B}_{\mathrm{IP}} \| \mathbf{I}$ [$\theta = 0°$, Fig. 2(f)]. As $\mathbf{B}_{\mathrm{IP}}$ is continuously rotated, inductance measurements provide a tomography of the order parameter in the vicinity of the vortex center, as shown in Fig. 2(b). The effect is remarkably robust: for $B_{\mathrm{IP}} = 1$ T, $k_{\perp}$ and $k_{\parallel}$ increase by a factor 7.66 and 1.64, respectively, compared to the $B_{\mathrm{IP}} = 0$ case, as deduced from the corresponding reduction of L_v in Fig. 2(a), red (blue) curve.

Now we turn to possible explanations for the striking observations in Fig. 2. The key findings that must be captured by a theoretical model are (i) the vortex inductance anomalously decreases with the applied in-plane field, (ii) the decrease is anisotropic, with a twofold symmetry, (iii) it is maximal (minimal) when the field is perpendicular (parallel) to the current density, and (iv) the effect is visible only in epitaxial Al/InAs 2DEG devices, while it is absent in the control Al/GaAs samples without 2DEG and with largely reduced SOI.

The noncentrosymmetry of the quasi-2D film is captured on the microscopic level by the isotropic Rashba Hamiltonian $H_R = \alpha_R(\mathbf{k} \times \mathbf{n}) \cdot \boldsymbol{\sigma}$, where the unit vector $\mathbf{n}$ (along the polar axis) is normal to the plane of the superconducting film. We estimate the Rashba coupling α_R and the g factor in the Zeeman Hamiltonian $H_Z = g\mu_B \mathbf{B} \cdot \boldsymbol{\sigma}$ to be of the order of $\alpha_R = 15$ meVnm and $g = -10$, respectively.

On the other hand, as shown by Edelstein [49], the joint effect of the Rashba SOI, in-plane magnetic field and superconducting pairing can be described, within the Ginzburg-Landau approach, by adding a new term to the free energy—the so-called Lifshitz invariant. As discussed below, it is the Lifshitz term which can explain the anisotropic vortex squeezing, in combination with the in-plane field. The Ginzburg-Landau free-energy density in question has the following form:

$$F[\Psi, \mathbf{A}] = a(T)|\Psi|^2 + \frac{b}{2}|\Psi|^4 + \frac{|\mathbf{D}\Psi|^2}{4m} + \frac{\mathbf{B}^2}{2\mu_0} + F_L[\Psi, \mathbf{A}], \tag{2}$$

where the last two terms correspond to the magnetic energy density and to the (isotropic) Lifshitz invariant [49]:

$$F_L[\Psi, \mathbf{A}] = -\frac{1}{2}\kappa(\mathbf{n} \times \mathbf{B}) \cdot [(\Psi)^* \mathbf{D}\Psi + \Psi(\mathbf{D}\Psi)^*]. \tag{3}$$

The Lifshitz invariant is the direct manifestation of Rashba SOI at the Ginzburg-Landau level. In the above expressions Ψ stands for the condensate wave function, $\mathbf{A}$ for the vector potential, $\mathbf{B} = \mathrm{rot}\mathbf{A}$ for the corresponding (in-plane plus out-of-plane) magnetic field, and $\mathbf{D} = (\hbar/i)\boldsymbol{\nabla} - 2e\mathbf{A}$ for the covariant momentum operator ($|e|$ is the elementary charge). Here and below we assume Rashba SOI with (at least) C_{4v} point-group symmetry in the sample plane. The whole symmetry of $F[\Psi, \mathbf{A}]$ is, however, lowered to C_{2v} when the in-plane magnetic field and current drive are present.

On the phenomenological level, a figure of merit quantifying the impact of the noncentrosymmetry is given by the parameter κ or the Lifshitz-Edelstein length ℓ_κ:

$$\kappa \simeq 3\frac{\alpha_R}{\hbar}\frac{g\mu_B}{v_F p_F}, \qquad \ell_\kappa = \frac{b}{2|\kappa|\mu_0|e|a(T)}, \tag{4}$$

where μ_B is the Bohr magneton, and p_F and v_F stand for the Fermi momentum and velocity (for a complete derivation, including the numerical prefactor, see Ref. [49]). Upon functional variation of the extended Ginzburg-Landau free-energy density $F[\Psi, \mathbf{A}]$, one obtains the first and second Ginzburg-Landau equation for 2D Rashba superconductor, as discussed in the Supplemental Material [66].

The goal of our analytical calculation is to obtain the wave function of the vortex order parameter $\Psi_v(x, y)$ in the vicinity of the vortex core at $(x_0 = 0, y_0 = 0)$; therefore, we assume the following asymptotic form,

$$\Psi_v(x, y) = (x + i\delta y)K \exp\left[\frac{p}{2}x^2 + qxy + \frac{r}{2}y^2\right], \tag{5}$$

where the real parameters K, δ, p, q, and r can be determined [66] from the Ginzburg-Landau equations including the Lifshitz term [69]. Obviously, for $\delta \neq 1$ the vortex factor $K \cdot (x + i\delta y)$ of the solution $\Psi_v(\mathrm{x}, \mathrm{y})$ possesses a certain ellipticity mimicking the reduction of symmetry to C_{2v} due to an in-plane magnetic field. When discussing the model, it is customary to assume a fixed direction of $\mathbf{B}_{\mathrm{IP}} \| \hat{\mathbf{y}}$, while in the experiment it is the direction of current that is kept fixed $\mathbf{I} \| \hat{\mathbf{x}}$. In the limit of a pointlike pinning defect, the effective vortex potential $U(x, y)$ mirrors $|\Psi_v(x, y)|^2$; hence,

$$U(x, y) \equiv \frac{1}{2}k_x x^2 + \frac{1}{2}k_y y^2 \simeq |\Psi_v(x, y)|^2 \simeq K^2 x^2 + K^2\delta^2 y^2. \tag{6}$$

The theoretical values of the curvatures $k_x = \partial_x^2 U(0, 0) \simeq 2K^2$ and $k_y = \partial_y^2 U(0, 0) \simeq 2K^2\delta^2$ of $U(x, y)$ can be directly linked to the experimentally determined curvatures (inductances) $k_{\parallel}(L_{v,\parallel})$ and $k_{\perp}(L_{v,\perp})$, where the subscripts $\parallel$ and $\perp$ discriminate correspondingly between the mutual orientations of $\mathbf{B}_{\mathrm{IP}}$ and $\mathbf{I}$ in the experiment, particularly,

$k_{\parallel} = k_x$ and $k_{\perp} = k_y$. The independently measured input parameters for our model are $\xi = 73$ nm, $\lambda = 227$ nm, and $B_z = 10$ mT. Theory provides a set of algebraic equations for k_x and k_y as functions of B_{IP}. The equations contain the Lifshitz-Edelstein length ℓ_κ and the effective thermodynamic critical field B_c^* as parameters that can be determined by fitting data in Fig. 2(a), using Eq. (1) to link curvature to inductance. Restricting the fit to the range of $[-0.1\ \mathrm{T}, 0.1\ \mathrm{T}]$ we obtain [66] $B_c^* = 96$ mT and $\ell_\kappa = 590$ nm. The resulting fitting curves are shown as solid lines in Fig. 2(a). Despite the simplified phenomenological approach, our model quantitatively captures (i) the increase of *both* curvatures, $k_{\parallel}$ and $k_{\perp}$, upon application of an in-plane field, as well as (ii) the anisotropy ratio $k_{\perp}/k_{\parallel} > 1$ of the two curvatures. For $B_{\mathrm{IP}} > 0.1$ T the fits underestimate L_v, most probably because the quadratic approximation of $\Psi(\mathbf{r})$ at the vortex cores is no longer valid.

In order to further substantiate our interpretation of the reduced vortex inductance as an enhanced pinning strength, we investigate an entirely different signature of pinning, i.e., the depinning critical current. If the local minima of $U(\mathbf{r})$ become sharper in in-plane field, then one would expect that not only its bottom curvature will increase, but also its maximal slope, i.e., $\max[|\partial_{\mathbf{r}} U(\mathbf{r})|]$. This corresponds to the maximal restoring force that pinning centers can exert before the depinning point. On the basis of the vortex inductance measurements just discussed, the depinning current is expected to display a similar peculiar increase with the in-plane field. We performed such measurements on a separate sample from the same wafer that was designed in a standard Hall bar geometry. The width was reduced to 2.3 μm, leading to a smaller critical current and thus less Joule heating.

Owing to the large contact resistance of this particular sample, a large heat is generated at the bonding pads of the device which reaches the device through the substrate in a fraction of a second. Therefore, the current-voltage characteristics (IVs) traces were acquired in 9 ms, with 30 s waiting time needed to cool the system back to the base temperature $T = 0.1$ K. The sweep time was chosen in such a way that a further reduction of the sweep time did not affect the depinning current anymore. Each measurement point corresponds to the average of the depinning currents resulting from 45 repetitions of the IVs.

The results of these depinning current measurements for $B_z = 5$ mT are shown in Fig. 3(a). To maximize the effect, the in-plane field is oriented perpendicular to the current. ($\mathbf{B}_{\mathrm{IP}} = B_y \hat{\mathbf{y}}$, $\theta = 90°$). We observe a minimum for the depinning current at zero in-plane field, a maximum at about $|B_y| \approx 60$ mT, and then eventually a rapid suppression for $|B_y| > 100$ mT, when pair breaking becomes significant. Figure 3(b) shows selected histograms for the depinning current distribution corresponding to selected values of B_y. The distributions are relatively narrow: the

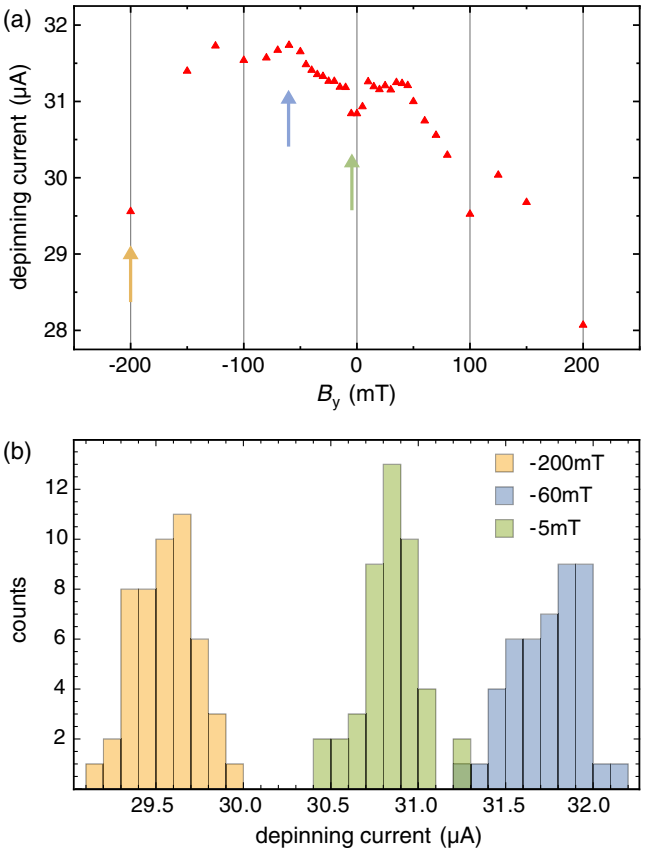

FIG. 3. dc transport signature of the field-enhanced pinning. (a) Depinning current as a function of the in-plane magnetic field component perpendicular to the current (B_y), measured for $B_z = 5$ mT. Each data point is obtained from the average of 45 repeated IV measurements. (b) Histograms showing the distribution of the depinning current values for three selected values of B_y, namely, -5 mT (light green), -60 mT (light blue), and -200 mT (light orange). These values are indicated by arrows of the corresponding colors in the top panel.

data scatter is mostly due to the extreme sensitivity of the measurement to the precise value of the effective B_z, which we kept constant at 5 mT using a field compensation routine, discussed in the Supplemental Material [66]. Further measurements on the same and on another device are discussed in the Supplemental Material [66]. These results confirm the outcome of the vortex inductance measurements; i.e., the pinning interaction is anisotropically enhanced by a moderate magnetic field. Hence, the depinning current provides a further independent evidence of the apparently anomalous shrinking of the vortex cores.

Before concluding, we want to briefly discuss alternative (or additional) mechanisms that might be responsible for the anisotropic vortex inductance in 2D Rashba superconductors. The simplest possible origin of anisotropy in $U(\mathbf{r})$ is through a magnetic field-induced anisotropy in the coherence length ξ, e.g., by an anisotropic Fermi velocity. The Rashba SOI spin splits the Fermi surface while

preserving its circular symmetry. An applied in-plane magnetic field shifts and distorts the two circular Fermi surfaces. However, for a realistic Rashba coefficient $\alpha_R = 15$ meV nm [29], we obtain a relative anisotropy in v_F of the order of just 10^{-3}, too small to explain the marked anisotropy observed in the experiment. Moreover, the measured anisotropy of the in-plane critical field [66] is also much smaller than that of L_v.

Another interesting possibility is that in an InAs 2DEG proximitized by an epitaxial Al layer the pairing function is not purely of s-wave type, but rather admixed of $p_x + ip_y$ wave. Without an in-plane field, the modulus of the pairing function is still isotropic both in the reciprocal and in the real space. The application of an in-plane field gradually projects the $p_x + ip_y$-wave pairing into its p_y-wave component. The anisotropic $\Delta(\mathbf{k})$ produces, upon Fourier transform, an anisotropic coherence length ξ. This argument does not explain, *per se*, the increase in the pinning force with the magnetic field. However, Hayashi and Kato [71,72] have found that for sharp defects (in the sense discussed in Ref. [73]) and for $p_x + ip_y$-wave pairing, the pinning potential becomes steeper near the vortex core center. Nevertheless, this picture cannot adequately explain the rapid decrease of the vortex inductance with small or moderate in-plane fields. We therefore believe that our model based on the Lifshitz invariant provides a more natural explanation of both the pinning enhancement and the field-induced anisotropy. On the other hand, our work is compatible with the occurrence of $p_x + ip_y$-wave pairing. The latter is at the basis of many proposals aiming at implementing topological superconductivity in InAs 2DEG proximitized by epitaxial Al. Recent experiments indicate that unconventional pairing affects the kinetic inductance in such systems [9]. Our data evidence the caveat that, in the presence of residual vortices, the inductance resulting from their oscillations around pinning centers can dominate over any other inductance contribution.

In conclusion, we have demonstrated experimentally that in 2D Rashba superconductors the application of an in-plane field squeezes the vortex cores, leading to an enhanced pinning. The vortex squeezing is anisotropic—vortex cores are more compressed if the in-plane magnetic field is orientated perpendicular to the supercurrent. By rotating the in-plane field, the inductance measurements provide a tomography of order parameter profile near the vortex core. These results constitute a clear manifestation of Lifshitz invariants in a macroscopic observable of a synthetic Rashba superconductor. Similar to skyrmions and chiral solitons [74–76] in magnetic systems with Lifshitz invariants, also Abrikosov vortices are strongly affected by the broken symmetries. Moreover, our study opens the path toward the manipulation of quasiparticles in the vortex cores [77] including Majorana fermions [78].

We thank A. Drachmann and C. Marcus for providing chips with Al/GaAs reference films and T. Lemberger, J. Schmalian, E. Bauer, M. Sigrist, D. Agterberg, Y. Ando, L. Tosi, and C. Timm for helpful discussions. Work at Regensburg University was funded by the Deutsche Forschungsgemeinschaft (DFG, German Research Foundation)—Project-ID 314695032–SFB 1277 (Subprojects B05, B07, and B08). D. K. acknowledges a partial support from the Project IM-2021-26 (SUPERSPIN) funded by Slovak Academy of Sciences via the program IMPULZ 2021.

The authors declare no competing interests.

[1] P. A. Frigeri, D. F. Agterberg, A. Koga, and M. Sigrist, *Superconductivity without Inversion Symmetry: MnSi versus* $CePt_3Si$, Phys. Rev. Lett. **92**, 097001 (2004).

[2] E. Bauer and M. Sigrist, in *Non-Centrosymmetric Superconductors*, edited by E. Bauer and M. Sigrist, Lecture Notes in Physics Vol. 847 (Springer, Berlin, 2012).

[3] M. Smidman, M. B. Salamon, H. Q. Yuan, and D. F. Agterberg, *Superconductivity and Spin–Orbit Coupling in Non-Centrosymmetric Materials: A Review*, Rep. Prog. Phys. **80**, 036501 (2017).

[4] V. M. Edelstein, *Characteristics of the Cooper Pairing in Two-Dimensional Noncentrosymmetric Electron Systems*, Sov. Phys. JETP **68**, 1244 (1989), http://jetp.ras.ru/cgi-bin/e/index/e/68/6/p1244?a=list.

[5] L. P. Gor'kov and E. I. Rashba, *Superconducting 2D System with Lifted Spin Degeneracy: Mixed Singlet-Triplet State*, Phys. Rev. Lett. **87**, 037004 (2001).

[6] L. Fu and C. L. Kane, *Superconducting Proximity Effect and Majorana Fermions at the Surface of a Topological Insulator*, Phys. Rev. Lett. **100**, 096407 (2008).

[7] S. Fujimoto, *Topological Order and Non-Abelian Statistics in Noncentrosymmetric s-Wave Superconductors*, Phys. Rev. B **77**, 220501(R) (2008).

[8] C. Zhang, S. Tewari, R. M. Lutchyn, and S. Das Sarma, $p_x + ip_y$ *Superfluid from s-Wave Interactions of Fermionic Cold Atoms*, Phys. Rev. Lett. **101**, 160401 (2008).

[9] D. Phan, J. Senior, A. Ghazaryan, M. Hatefipour, W. M. Strickland, J. Shabani, M. Serbyn, and A. P. Higginbotham, *Detecting Induced* $p \pm ip$ *Pairing at the Al-InAs Interface with a Quantum Microwave Circuit*, Phys. Rev. Lett. **128**, 107701 (2022).

[10] X. Xi, Z. Wang, W. Zhao, J.-H. Park, K. T. Law, H. Berger, L. Forró, J. Shan, and K. F. Mak, *Ising Pairing in Superconducting* $NbSe_2$ *Atomic Layers*, Nat. Phys. **12**, 139 (2016).

[11] J. M. Lu, O. Zheliuk, I. Leermakers, N. F. Q. Yuan, U. Zeitler, K. T. Law, and J. T. Ye, *Evidence for Two-Dimensional Ising Superconductivity in Gated* MoS_2, Science **350**, 1353 (2015).

[12] R. Wakatsuki, Y. Saito, S. Hoshino, Y. M. Itahashi, T. Ideue, M. Ezawa, Y. Iwasa, and N. Nagaosa, *Nonreciprocal Charge Transport in Noncentrosymmetric Superconductors*, Sci. Adv. **3**, e1602390 (2017).

[13] T. Ideue, K. Hamamoto, S. Koshikawa, M. Ezawa, S. Shimizu, Y. Kaneko, Y. Tokura, N. Nagaosa, and Y. Iwasa, *Bulk Rectification Effect in a Polar Semiconductor*, Nat. Phys. **13**, 578 (2017).

[14] Y. M. Itahashi, T. Ideue, Y. Saito, S. Shimizu, T. Ouchi, T. Nojima, and Y. Iwasa, *Nonreciprocal Transport in Gate-Induced Polar Superconductor SrTiO3*, Sci. Adv. **6**, eaay9120 (2020).

[15] S. Hoshino, R. Wakatsuki, K. Hamamoto, and N. Nagaosa, *Nonreciprocal Charge Transport in Two-Dimensional Noncentrosymmetric Superconductors*, Phys. Rev. B **98**, 054510 (2018).

[16] Y. Tokura and N. Nagaosa, *Nonreciprocal Responses from Non-Centrosymmetric Quantum Materials*, Nat. Commun. **9**, 3740 (2018).

[17] E. V. Bezuglyi, A. S. Rozhavsky, I. D. Vagner, and P. Wyder, *Combined Effect of Zeeman Splitting and Spin-Orbit Interaction on the Josephson Current in a Superconductor–Two-Dimensional Electron Gas–Superconductor Structure*, Phys. Rev. B **66**, 052508 (2002).

[18] A. Buzdin, *Direct Coupling between Magnetism and Superconducting Current in the Josephson φ_0 Junction*, Phys. Rev. Lett. **101**, 107005 (2008).

[19] A. A. Reynoso, G. Usaj, C. A. Balseiro, D. Feinberg, and M. Avignon, *Anomalous Josephson Current in Junctions with Spin Polarizing Quantum Point Contacts*, Phys. Rev. Lett. **101**, 107001 (2008).

[20] A. A. Reynoso, G. Usaj, C. A. Balseiro, D. Feinberg, and M. Avignon, *Spin-Orbit-Induced Chirality of Andreev States in Josephson Junctions*, Phys. Rev. B **86**, 214519 (2012).

[21] T. Yokoyama, M. Eto, and Y. V. Nazarov, *Anomalous Josephson Effect Induced by Spin-Orbit Interaction and Zeeman Effect in Semiconductor Nanowires*, Phys. Rev. B **89**, 195407 (2014).

[22] K. Shen, G. Vignale, and R. Raimondi, *Microscopic Theory of the Inverse Edelstein Effect*, Phys. Rev. Lett. **112**, 096601 (2014).

[23] F. Konschelle, I. V. Tokatly, and F. S. Bergeret, *Theory of the Spin-Galvanic Effect and the Anomalous Phase Shift φ_0 in Superconductors and Josephson Junctions with Iintrinsic Spin-Orbit Coupling*, Phys. Rev. B **92**, 125443 (2015).

[24] D. B. Szombati, S. Nadj-Perge, D. Car, S. R. Plissard, E. P. A. M. Bakkers, and L. P. Kouwenhoven, *Josephson ϕ_0-Junction in Nanowire Quantum Dots*, Nat. Phys. **12**, 568 (2016).

[25] A. Assouline, C. Feuillet-Palma, N. Bergeal, T. Zhang, A. Mottaghizadeh, A. Zimmers, E. Lhuillier, M. Eddrie, P. Atkinson, M. Aprili, and H. Aubin, *Spin-Orbit Induced Phase-Shift in Bi_2Se_3 Josephson Junctions*, Nat. Commun. **10**, 126 (2019).

[26] W. Mayer, M. C. Dartiailh, J. Yuan, K. S. Wickramasinghe, E. Rossi, and J. Shabani, *Gate Controlled Anomalous Phase Shift in Al/InAs Josephson Junctions*, Nat. Commun. **11**, 212 (2020).

[27] E. Strambini, A. Iorio, O. Durante, R. Citro, C. Sanz-Fernández, C. Guarcello, I. V. Tokatly, A. Braggio, M. Rocci, N. Ligato, V. Zannier, L. Sorba, F. S. Bergeret, and F. Giazotto, *A Josephson Phase Battery*, Nat. Nanotechnol. **15**, 656 (2020).

[28] F. Ando, Y. Miyasaka, T. Li, J. Ishizuka, T. Arakawa, Y. Shiota, T. Moriyama, Y. Yanase, and T. Ono, *Observation of Superconducting Diode Effect*, Nature (London) **584**, 373 (2020).

[29] C. Baumgartner, L. Fuchs, A. Costa, S. Reinhardt, S. Gronin, G. C. Gardner, T. Lindemann, M. J. Manfra, P. E. Faria Junior, D. Kochan, J. Fabian, N. Paradiso, and C. Strunk, *Supercurrent Rectification and Magnetochiral Effects in Symmetric Josephson Junctions*, Nat. Nanotechnol. **17**, 39 (2022).

[30] C. Baumgartner, L. Fuchs, A. Costa, J. P. Cortes, S. Reinhardt, S. Gronin, G. C. Gardner, T. Lindemann, M. J. Manfra, P. E. Faria-Junior, D. Kochan, J. Fabian, N. Paradiso, and C. Strunk, *Effect of Rashba and Dresselhaus Spin-Orbit Coupling on Supercurrent Rectification and Magnetochiral Anisotropy of Ballistic Josephson Junctions*, J. Phys. Condens. Matter **34**, 154005 (2022).

[31] J. Alicea, *Majorana Fermions in a Tunable Semiconductor Device*, Phys. Rev. B **81**, 125318 (2010).

[32] P. He, S. M. Walker, Steven S.-L. Zhang, F. Y. Bruno, M. S. Bahramy, J. M. Lee, R. Ramaswamy, K. Cai, O. Heinonen, G. Vignale, F. Baumberger, and H. Yang, *Observation of Out-of-Plane Spin Texture in a $SrTiO_3(111)$ Two-Dimensional Electron Gas*, Phys. Rev. Lett. **120**, 266802 (2018).

[33] D. Shaffer, J. Kang, F. J. Burnell, and R. M. Fernandes, *Crystalline Nodal Topological Superconductivity and Bogolyubov Fermi Surfaces in Monolayer $NbSe_2$*, Phys. Rev. B **101**, 224503 (2020).

[34] V. Mineev and K. V. Samokhin, *Helical Phases in Superconductors*, J. Exp. Theor. Phys. **78**, 401 (1994), http://jetp.ras.ru/cgi-bin/e/index/e/78/3/p401?a=list.

[35] Y. Yanase and M. Sigrist, *Helical Superconductivity in Non-Centrosymmetric Superconductors with Dominantly Spin Triplet Pairing*, J. Phys. Soc. Jpn. **77**, 342 (2008).

[36] D. Agterberg, *Novel Magnetic Field Effects in Unconventional Superconductors*, Physica (Amsterdam) **387C**, 13 (2003).

[37] J. Shabani, M. Kjaergaard, H. J. Suominen, Y. Kim, F. Nichele, K. Pakrouski, T. Stankevic, R. M. Lutchyn, P. Krogstrup, R. Feidenhans'l, S. Kraemer, C. Nayak, M. Troyer, C. M. Marcus, and C. J. Palmstrøm, *Two-Dimensional Epitaxial Superconductor-Semiconductor Heterostructures: A Platform for Topological Superconducting Networks*, Phys. Rev. B **93**, 155402 (2016).

[38] M. Kjaergaard, F. Nichele, H. J. Suominen, M. P. Nowak, M. Wimmer, A. R. Akhmerov, J. A. Folk, K. Flensberg, J. Shabani, C. J. Palmstrøm, and C. M. Marcus, *Quantized Conductance Doubling and Hard Gap in a Two-Dimensional Semiconductor–Superconductor Heterostructure*, Nat. Commun. **7**, 12841 (2016).

[39] M. Kjaergaard, H. J. Suominen, M. P. Nowak, A. R. Akhmerov, J. Shabani, C. J. Palmstrøm, F. Nichele, and C. M. Marcus, *Transparent Semiconductor-Superconductor Interface and Induced Gap in an Epitaxial Heterostructure Josephson Junction*, Phys. Rev. Appl. **7**, 034029 (2017).

[40] W. Mayer, J. Yuan, K. S. Wickramasinghe, T. Nguyen, M. C. Dartiailh, and J. Shabani, *Superconducting Proximity Effect in Epitaxial Al-InAs Heterostructures*, Appl. Phys. Lett. **114**, 103104 (2019).

[41] A. C. Potter and P. A. Lee, *Engineering a $p+ip$ Superconductor: Comparison of Topological Insulator and Rashba Spin-Orbit-Coupled Materials*, Phys. Rev. B **83**, 184520 (2011).

[42] M. Hell, K. Flensberg, and M. Leijnse, *Coupling and Braiding Majorana Bound States in Networks Defined in Two-Dimensional Electron Gases with Proximity-Induced Superconductivity*, Phys. Rev. B **96**, 035444 (2017).

[43] M. Hell, M. Leijnse, and K. Flensberg, *Two-Dimensional Platform for Networks of Majorana Bound States*, Phys. Rev. Lett. **118**, 107701 (2017).

[44] H. J. Suominen, M. Kjaergaard, A. R. Hamilton, J. Shabani, C. J. Palmstrøm, C. M. Marcus, and F. Nichele, *Zero-Energy Modes from Coalescing Andreev States in a Two-Dimensional Semiconductor-Superconductor Hybrid Platform*, Phys. Rev. Lett. **119**, 176805 (2017).

[45] F. Nichele, A. C. C. Drachmann, A. M. Whiticar, E. C. T. O'Farrell, H. J. Suominen, A. Fornieri, T. Wang, G. C. Gardner, C. Thomas, A. T. Hatke, P. Krogstrup, M. J. Manfra, K. Flensberg, and C. M. Marcus, *Scaling of Majorana Zero-Bias Conductance Peaks*, Phys. Rev. Lett. **119**, 136803 (2017).

[46] F. Pientka, A. Keselman, E. Berg, A. Yacoby, A. Stern, and B. I. Halperin, *Topological Superconductivity in a Planar Josephson Junction*, Phys. Rev. X **7**, 021032 (2017).

[47] J. S. Lee, B. Shojaei, M. Pendharkar, A. P. McFadden, Y. Kim, H. J. Suominen, M. Kjaergaard, F. Nichele, H. Zhang, C. M. Marcus, and C. J. Palmstrøm, *Transport Studies of Epi-*Al/InAs *Two-Dimensional Electron Gas Systems for Required Building-Blocks in Topological Superconductor Networks*, Nano Lett. **19**, 3083 (2019).

[48] A. Fornieri, A. M. Whiticar, F. Setiawan, E. Portolés, A. C. C. Drachmann, A. Keselman, S. Gronin, C. Thomas, T. Wang, R. Kallaher, G. C. Gardner, E. Berg, M. J. Manfra, A. Stern, C. M. Marcus, and F. Nichele, *Evidence of Topological Superconductivity in Planar Josephson Junctions*, Nature (London) **569**, 89 (2019).

[49] V. M. Edelstein, *The Ginzburg-Landau Equation for Superconductors of Polar Symmetry*, J. Phys. Condens. Matter **8**, 339 (1996).

[50] V. P. Mineev and K. V. Samokhin, *Nonuniform States in Noncentrosymmetric Superconductors: Derivation of Lifshitz Invariants from Microscopic Theory*, Phys. Rev. B **78**, 144503 (2008).

[51] V. M. Edelstein, *Magnetoelectric Effect in Polar Superconductors*, Phys. Rev. Lett. **75**, 2004 (1995).

[52] S. Fujimoto, *Magnetoelectric Effects in Heavy-Fermion Superconductors without Inversion Symmetry*, Phys. Rev. B **72**, 024515 (2005).

[53] R. P. Kaur, D. F. Agterberg, and M. Sigrist, *Helical Vortex Phase in the Noncentrosymmetric* $CePt_3Si$, Phys. Rev. Lett. **94**, 137002 (2005).

[54] O. Dimitrova and M. V. Feigel'man, *Theory of a Two-Dimensional Superconductor with Broken Inversion Symmetry*, Phys. Rev. B **76**, 014522 (2007).

[55] D. F. Agterberg and R. P. Kaur, *Magnetic-Field-Induced Helical and Stripe Phases in Rashba Superconductors*, Phys. Rev. B **75**, 064511 (2007).

[56] L. S. Levitov, Y. V. Nazarov, and G. M. Eliashberg, *Magnetostatics of Superconductors without an Inversion Center*, JETP Lett. **41**, 445 (1985), http://jetpletters.ru/ps/1467/article_22366.shtml.

[57] S. K. Yip, *Magnetic Properties of a Superconductor with No Inversion Symmetry*, J. Low Temp. Phys. **140**, 67 (2005).

[58] A. S. Cameron, Y. S. Yerin, Y. V. Tymoshenko, P. Y. Portnichenko, A. S. Sukhanov, M. C. Hatnean, D. M. K. Paul, G. Balakrishnan, R. Cubitt, A. Heinemann, and D. S. Inosov, *Rotation of the Magnetic Vortex Lattice in* Ru_7B_3 *Driven by the Effects of Broken Time-Reversal and Inversion Symmetry*, Phys. Rev. B **100**, 024518 (2019).

[59] More precisely, the free energy is a convolution of the defect's pinning potential with the profile of $|\Psi(x,y)|^2$ [60].

[60] G. Blatter, M. V. Feigel'man, V. B. Geshkenbein, A. I. Larkin, and V. M. Vinokur, *Vortices in High-Temperature Superconductors*, Rev. Mod. Phys. **66**, 1125 (1994).

[61] Note that in the literature one often finds a related quantity, the so-called Labusch parameter $k_p = k/d$, where d stands for the film thickness [62,63].

[62] M. R. Beasley, R. Labusch, and W. W. Webb, *Flux Creep in Type-II Superconductors*, Phys. Rev. **181**, 682 (1969).

[63] M. Golosovsky, M. Tsindlekht, and D. Davidov, *Radio-Frequency Resistance in the Mixed State for Subcritical Currents*, Supercond. Sci. Technol. **9**, 1 (1996).

[64] J. I. Gittleman and B. Rosenblum, *Radio-Frequency Resistance in the Mixed State for Subcritical Currents*, Phys. Rev. Lett. **16**, 734 (1966).

[65] C. Baumgartner, L. Fuchs, L. Frész, S. Reinhardt, S. Gronin, G. C. Gardner, M. J. Manfra, N. Paradiso, and C. Strunk, *Josephson Inductance as a Probe for Highly Ballistic Semiconductor-Superconductor Weak Links*, Phys. Rev. Lett. **126**, 037001 (2021).

[66] See Supplemental Material at http://link.aps.org/supplemental/10.1103/PhysRevX.12.041020 for further details.

[67] Even a few ohms of ac resistance (4 orders of magnitude less than R_N) damp the resonance Q factor below unity.

[68] It is worth stressing that, at least in our setup, the measurement of a pure kinetic inductance versus B_z is difficult on macroscopic devices: on a millimeter scale, it is not possible to perfectly zero the out-of-plane field everywhere on the sample owing to the unavoidable inhomogeneity of the compensation field. The residual B_z locally introduces vortices that have a sizable inductance which adds to the pure kinetic inductance.

[69] The ansatz for $\Psi_v(x,y)$ has the same asymptotic form (including the cubic terms for the vortex core region, i.e., for $x/\xi, y/\xi \ll 1$) as the Abrikosov solution in the conventional case [70].

[70] A. A. Abrikosov, *On the Magnetic Properties of Superconductors of the Second Group*, ZhETF **32**, 1442 (1957) [J. Exp. Theor. Phys. **5**, 1174 (1957)], http://jetp.ras.ru/cgi-bin/e/index/e/5/6/p1174?a=list.

[71] N. Hayashi and Y. Kato, *Elementary Vortex Pinning Potential in a Chiral p-Wave Superconductor*, Phys. Rev. B **66**, 132511 (2002).

[72] Y. Kato and N. Hayashi, *Physics of Vortex Core in Chiral p-Wave Superconductor*, Physica (Amsterdam) **388-389C**, 519 (2003).

[73] E. V. Thuneberg, J. Kurkijärvi, and D. Rainer, *Elementary-Flux-Pinning Potential in Type-II Superconductors*, Phys. Rev. B **29**, 3913 (1984).

[74] A. Fert, N. Reyren, and V. Cros, *Magnetic Skyrmions: Advances in Physics and Potential Applications*, Nat. Rev. Mater. **2**, 17031 (2017).

[75] A. N. Bogdanov and C. Panagopoulos, *Physical Foundations and Basic Properties of Magnetic Skyrmions*, Nat. Rev. Phys. **2**, 492 (2020).

[76] B. Göbel, I. Mertig, and O. A. Tretiakov, *Beyond Skyrmions: Review and Perspectives of Alternative Magnetic Quasiparticles*, Phys. Rep. **895**, 1 (2021).

[77] C. Caroli, P. De Gennes, and J. Matricon, *Bound Fermion States on a Vortex Line in a Type II Superconductor*, Phys. Lett. **9**, 307 (1964).

[78] J.-P. Xu, M.-X. Wang, Z. L. Liu, J.-F. Ge, X. Yang, C. Liu, Z. A. Xu, D. Guan, C. L. Gao, D. Qian, Y. Liu, Q.-H. Wang, F.-C. Zhang, Q.-K. Xue, and J.-F. Jia, *Experimental Detection of a Majorana Mode in the Core of a Magnetic Vortex inside a Topological Insulator-Superconductor* $Bi_2Te_3/NbSe_2$ *Heterostructure*, Phys. Rev. Lett. **114**, 017001 (2015).